© 2020. Published by The Company of Biologists Ltd | Journal of Cell Science (2020) 133, jcs244657. doi:10.1242/jcs.244657

RESEARCH ARTICLE

Proteomic analysis reveals the direct recruitment of intrinsically disordered regions to stress granules in *S. cerevisiae*

Mang Zhu[1], Erich R. Kuechler[1], Joyce Zhang[1], Or Matalon[2], Benjamin Dubreuil[2], Analise Hofmann[3], Chris Loewen[3], Emmanuel D. Levy[2], Joerg Gsponer[1] and Thibault Mayor[1,*]

ABSTRACT

Stress granules (SGs) are stress-induced membraneless condensates that store non-translating mRNA and stalled translation initiation complexes. Although metazoan SGs are dynamic compartments where proteins can rapidly exchange with their surroundings, yeast SGs seem largely static. To gain a better understanding of yeast SGs, we identified proteins that sediment after heat shock using mass spectrometry. Proteins that sediment upon heat shock are biased toward a subset of abundant proteins that are significantly enriched in intrinsically disordered regions (IDRs). Heat-induced SG localization of over 80 proteins were confirmed using microscopy, including 32 proteins not previously known to localize to SGs. We found that several IDRs were sufficient to mediate SG recruitment. Moreover, the dynamic exchange of IDRs can be observed using fluorescence recovery after photobleaching, whereas other components remain immobile. Lastly, we showed that the IDR of the Ubp3 deubiquitinase was critical for yeast SG formation. This work shows that IDRs can be sufficient for SG incorporation, can remain dynamic in vitrified SGs, and can play an important role in cellular compartmentalization upon stress.

This article has an associated First Person interview with the first author of the paper.

KEY WORDS: Heat shock, Intrinsically disordered regions, Proteomic analysis, Stress granules, *Saccharomyces cerevisiae*

INTRODUCTION

Most organisms optimally grow over narrow temperature ranges, and small thermal fluctuations can lead to many detrimental effects (Richter et al., 2010). For instance, maintaining protein homeostasis during temperature changes presents a major challenge to cellular systems, because many polypeptides have marginally thermostable tertiary structures (Ghosh and Dill, 2010). To account for these instabilities, multiple mechanisms are in place to respond to heat stress. These can include, but are not limited to, transcriptional upregulation of heat shock proteins, inhibition of translation, and increased proteolysis. One part of the heat stress response in a wide range of organisms, from yeast and fly to mammals, is the formation of heat stress granules (SGs) (Farny et al., 2009; Grousl et al., 2009; Kedersha et al., 2005). SGs are membraneless ribonucleoprotein particles (RNPs) composed of mRNA and proteins. SGs assemble synchronously with the stalling of protein translation (Buchan and Parker, 2009; Jain et al., 2016; Khong et al., 2017) and function as storage sites for non-translating RNA and stalled translation initiation complexes (Fan and Leung, 2016; Kimball et al., 2003). Other roles of SGs, including the regulation of apoptosis, have also been shown (Thedieck et al., 2013). Importantly, impairment of SG regulation can have dramatic consequences. For instance, a recent study has shown that mutations of the SG protein FUS can affect its compartmentalization and lead to amyotrophic lateral sclerosis (ALS) or rare forms of frontotemporal lobar degeneration (FTLD) (Patel et al., 2015). Despite the growing understanding of SGs, further investigation is required to fully elucidate the composition, function, mechanisms of the formation, organization, and regulation of these membraneless compartments.

SG formation is hypothesized to be governed, in part, by a demixing process known as liquid–liquid phase separation (LLPS) (Alberti et al., 2019; Pak et al., 2016; Protter et al., 2018; Turoverov et al., 2019). Recent studies have shown that several SG proteins form droplets or hydrogels *in vitro* (Hyman et al., 2014; Lin et al., 2015; Molliex et al., 2015; Patel et al., 2015; Riback et al., 2017). For instance, the protein dynamics within mammalian SGs and the rapid, diffusive exchange of SG proteins with their surroundings, as measured by fluorescence recovery after photobleaching (FRAP), is consistent with LLPS and liquid droplet formation (Buchan and Parker, 2009). Intriguingly, indirect evidence suggests that yeast SGs appear to display a non-amyloid, solid-like state that is 1,6-hexanediol resistant but SDS soluble (Kroschwald et al., 2015). Such a difference in material properties of SGs between yeast and metazoans could be attributed to the presence of misfolded proteins in yeast SGs that reduce the mobility of other components (Cherkasov et al., 2013; Kroschwald et al., 2015). Supporting this notion, deletion of the Hsp104 disaggregase delays SG dissolution during heat stress recovery (Kroschwald et al., 2018, 2015). Interestingly, SGs in *Caenorhabditis elegans* become more solid-like in elderly animals indicating that, although yeast SGs are potentially distinct from their metazoan counterparts, the solid-like state gained during aging could be driven by similar mechanisms to those seen in yeast SG formation (Lechler et al., 2017). Additionally, it has been proposed that a dynamic shell may complete the SG structure (Buchan and Parker, 2009; Jain et al., 2016). This finding raises the questions of whether individual components contained in yeast SGs could remain mobile and why yeast SGs may display distinct physical properties from their mammalian counterparts.

Intrinsically disordered regions (IDRs) have been shown to be enriched in multiple membraneless compartments (Kuechler et al., 2020; Mittag and Parker, 2018; Youn et al., 2019). However, individual case studies show different roles for IDRs in LLPS. For instance, IDRs can enable promiscuous interactions in concert with specific domain interactions and, in some cases, have a more

[1]Michael Smith Laboratories, Department of Biochemistry and Molecular Biology, University of British Columbia, Vancouver, BC, Canada, V6T 1Z4. [2]Department of Structural Biology, Weizmann Institute of Science, Rehovot 7610001, Israel. [3]Department of Cellular and Physiological Sciences, University of British Columbia, Vancouver, BC, Canada, V6T 1Z3.

*Author for correspondence (mayor@msl.ubc.ca)

M.Z., 0000-0002-3177-5541; T.M., 0000-0002-9289-3939

Handling Editor: Maria Carmo-Fonseca
Received 30 January 2020; Accepted 15 May 2020

Journal of Cell Science (2020) 133, jcs244657. doi:10.1242/jcs.244657

dominant effect, such as those observed for prion-like domains in both TIA-1 and Lsm4 in SG formation and in yeast P-body formation, respectively (Decker et al., 2007; Gilks et al., 2004). In another case, the prion-like domain located within the IDR of Sup35 can phase separate *in vitro* and prevent aggregation to promote stress recovery *in vivo* (Franzmann et al., 2018). Other reports have shown that the presence of IDRs in proteins can weaken specific interactions, and those IDRs are not directly recruited to the P-body membraneless compartment *in vivo* (Protter et al., 2018). A comprehensive characterization of yeast SG composition and the roles of IDRs in these condensates will further our understanding of SG regulation and the involvement of SGs in diseases.

In this study, we identify yeast proteins that change their fractionation pattern upon heat stress. These proteins share many common features and include many novel SG-localizing proteins. We confirm using FRAP that several of these proteins are not dynamic once recruited into heat SGs. We then demonstrate that IDRs alone can, in several cases, be sufficient for SG recruitment. We characterize the role of two IDRs, and show that IDRs can undertake distinct roles: one IDR rapidly exchanged in and out of the stress-induced foci, whereas the other was required for SG formation. This work highlights the importance of IDRs in stress-induced protein compartmentalization and shows that, despite the more solid-like state of yeast SGs, some elements within this assembly remain highly dynamic.

RESULTS

Global identification of proteins prone to sedimentation after heat shock

Previously, we showed that long proteins with low-complexity IDRs are more 'pelletable' (i.e. have the ability to be enriched in the pellet after centrifugation) in unstressed eukaryotic cells (yeast, HeLa, and mouse brain tissue cells) (Albu et al., 2015). We used a similar approach here to delineate features of proteins that sediment under stress conditions. We performed a systems-wide analysis of *Saccharomyces cerevisiae* by combining stable isotope labeling by amino acids in cell culture (SILAC) with cell fractionation to identify proteins that become more pelletable after acute heat shock. Differentially labeled cells were either treated or not treated with heat shock at 45°C for 20 min, which induces a delay in growth without affecting viability (Fang et al., 2011). SILAC-labeled cells were subsequently mixed, lysed, and fractionated by centrifugation before mass spectrometry analysis (Fig. 1A). Among the 3734 proteins identified by at least two peptides in the supernatant fraction, 2717 proteins were quantified in three independent experiments (Fig. 1B; Table S1). The analysis showed that more than 60% of the quantified proteins remained predominately in the supernatant after heat shock. In contrast, a subset of 165 proteins showed a 90% or higher depletion from the supernatant after heat shock. Ola1 had the highest quantified depletion; with less than 2% of Ola1 remaining in the supernatant. In parallel, we identified 3528 proteins from the pellet fraction, among which 2558 proteins were quantified in all three experiments (Fig. 1C; Table S2). Most proteins quantified in both supernatant and pellet fractions displayed inversely correlated ratios consistent with the theoretical curve calculated based on the ratio change caused by the shift of protein from the supernatant fraction to the pellet fraction (Fig. 1D). However, a small group of proteins were depleted from both fractions after heat shock, possibly indicating these proteins are depleted from the cell after the stress. Protein localization analysis revealed that a majority of this protein group localize to the nucleus or nucleolus (Table S3). Analysis of the total cell lysate showed that expression levels of these proteins remained unchanged after heat shock (Fig. S1A). Therefore, it is likely these proteins form into compact structures or macro-molecular assemblies that are depleted following the removal of cell debris performed at low-speed centrifugation. To avoid omitting data from highly pelletable structures, we focused our analysis on proteins depleted from the supernatant.

Next, we compared our supernatant analysis with similar recent studies. Many proteins with a tenfold or more depletion from the supernatant (165 proteins) overlap with proteins known to aggregate or form cellular inclusions (Fig. S1B) (Cherkasov et al., 2015; Wallace et al., 2015). Nine of these proteins were previously classified as super-aggregators by Drummond and colleagues (Wallace et al., 2015) and many of these proteins (38 in total) have been shown to colocalize with the Pab1 stress granule marker after heat shock by Cherkasov et al. (2015). Gene ontology (GO) analysis showed that these highly pelletable proteins are enriched for cytosolic SG proteins (P=3.19×10^{-13}, count=22). To validate our approach, we sampled 13 candidate cytosolic proteins among those quantified by mass spectrometry to assess their localization upon heat shock when tagged with GFP. Candidate proteins that were found to be unaffected by heat shock during our supernatant analysis remained diffuse within the cell, whereas proteins that we determined to be depleted from the supernatant fraction displayed distinct puncta (Fig. S1C), indicating that these proteins are likely recruited to foci after acute heat shock. Importantly, most chaperone or co-chaperone proteins were found to remain in the supernatant fraction (Fig. S1D), presumably while associated to misfolded proteins that do not aggregate. Surprisingly, Sis1 Hsp40 remained predominately in the supernatant, despite having been shown previously to be recruited to deposits at amyloidic sites (Park et al., 2013). In contrast, the small heat shock proteins Hsp26 and Hsp42 were depleted, which is consistent with their reported association to stress-induced foci (Escusa-Toret et al., 2013; Specht et al., 2011). Additionally, many translation initiation factors and ribosome-associated chaperones (RACs) were depleted from the supernatant (Fig. S1D), consistent with previous studies (Cherkasov et al., 2015; Wallace et al., 2015). In a previous study, Groušl et al. (2009) showed that proteins from 40S ribosomal subunits were recruited into SGs upon heat shock; however, we did not observe depletion of these proteins from the supernatant, and selected small ribosomal subunits (Rps1B and Rps9A) did not form foci after heat shock (Fig. S1C). These results corroborate a report that ribosomal proteins do not prominently localize in yeast SGs (Cherkasov et al., 2013). In agreement with the latter report, all cytosolic ribosomal proteins identified in our study remained largely in the supernatant after heat shock.

Heat-induced pelletable proteins share common characteristics

To identify potential protein features correlated with increased 'pelletability' upon heat shock, we performed computational analysis comparing those proteins that mostly remained in the supernatant (hereafter called soluble; 1704 proteins) to those that were depleted from the supernatant (referred to here as pelletable; 1013 proteins) (Fig. 2A). The pelletable proteins have a significantly longer sequence length (Fig. 2B; n and P-values are reported in Table S4) and have a significantly depleted grand average of hydropathy (GRAVY) score, which is a measure of hydrophobicity (Fig. 2C). Correspondingly, these pelletable proteins are also composed of a significantly greater proportion of charged, both positively and negatively, residues (Fig. S2A–C). Additionally, these proteins were predicted to be significantly enriched in IDRs (Fig. 2D). In good agreement with these last three

Journal of Cell Science (2020) 133, jcs244657. doi:10.1242/jcs.244657

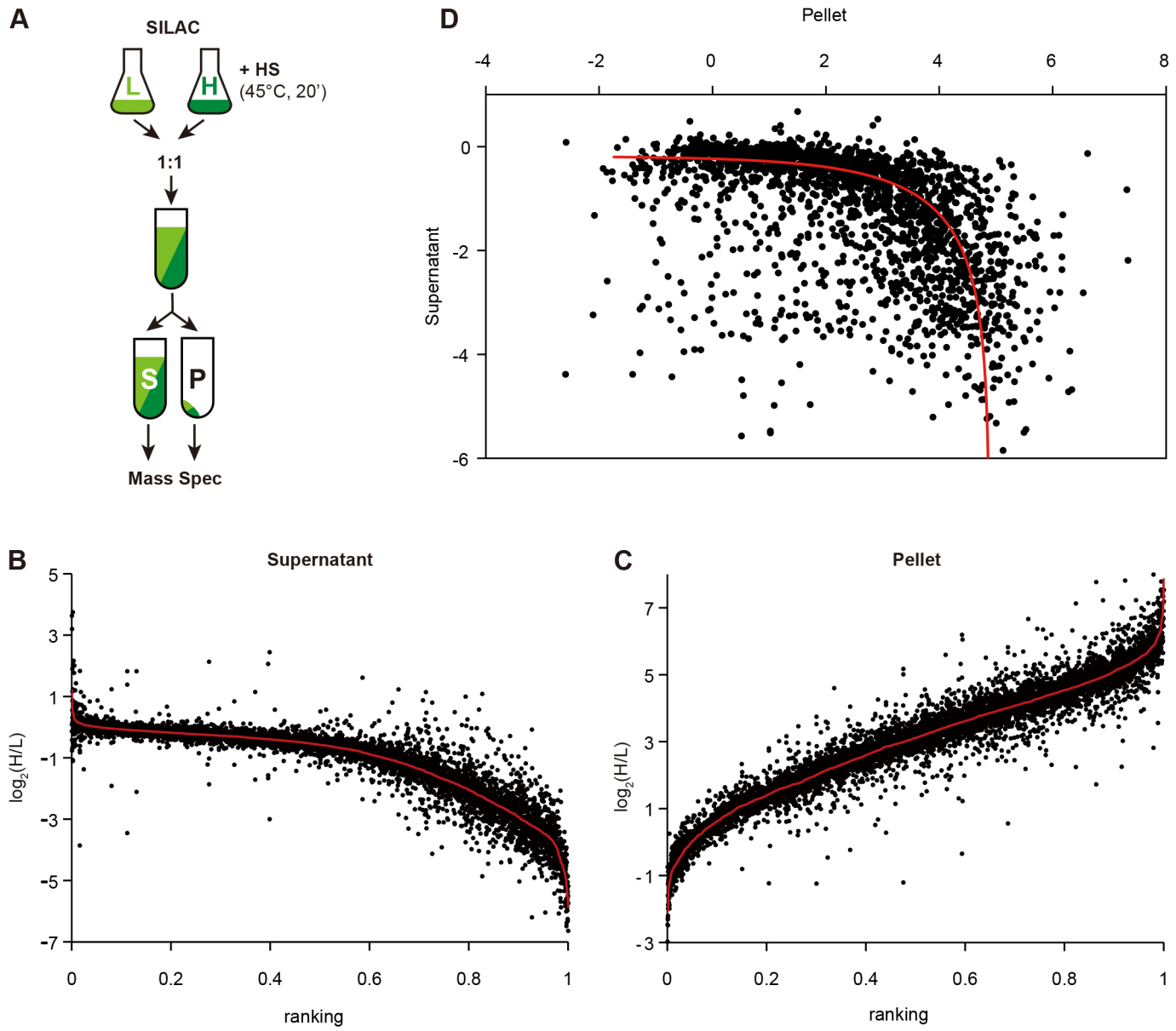

Fig. 1. Identification of pelletable proteins after heat shock by mass spectrometry. (A) Schematic of the SILAC mass spectrometry approach to identify pelletable proteins after heat shock (HS). L, light-labeled cells; H, heavy-labeled cells; S, supernatant; P, pellet. (B,C) Log_2 SILAC ratios (H/L) of proteins after and before heat shock in supernatant (B) and pellet (C) fractions. Proteins are ranked based on descending ratios, each black dot represents each protein in one of three analyses, and the red line marks the geometric mean of the three replicates. (D) Plot of the averaged log_2 ratio (H/L) of 2060 proteins quantified in both the pellet and supernatant fractions. Red line indicates the theoretical curve.

observations, pelletable proteins contained more predicted solvent-exposed residues (Fig. 2E). These results suggest that these proteins have more expanded structures with flexible IDRs that could facilitate transient interactions with other proteins or nucleic acids, which might facilitate their enrichment in the pellet fraction.

Because proteins that displayed greater pelletability after heat shock formed more distinct foci (Fig. S1C) and were enriched for SG proteins, we further separated pelletable proteins into three additional subgroups based on their fold depletion: group (I) 165 proteins depleted over tenfold; group (II) 287 proteins depleted between five- and ten-fold, and group (III) 561 proteins depleted between two- and five-fold (Fig. 2A; the cutoffs were selected without the assumption of their biological relevance). Upon initial examination of these groups, we found that group I was uniquely enriched for RGG motifs (25 proteins, *P*-value: 7.2×10^{-6}), which are known to aid in the formation of biological LLPS media and are implicated in SG formation (Chong et al., 2018). Surprisingly, proteins displaying over a ten-fold depletion from the supernatant (group I) were more abundant in comparison to other pelletable proteins (groups II and III; Fig. 2F). In addition, only proteins in that group displayed a significantly lower apparent melting temperatures (T_m) in comparison to soluble proteins (Fig. 2G). All other previously described features associated with pelletable proteins are also enriched in the three subgroups in comparison to soluble proteins (Fig. S2D–H). Given the fact that proteins in group I displayed higher protein abundances coupled with lower apparent melting temperatures, it suggests that protein pelletability is likely driven by specific characteristics that help regulate protein coalescence during the cellular stress response induced by heat shock.

Journal of Cell Science (2020) 133, jcs244657. doi:10.1242/jcs.244657

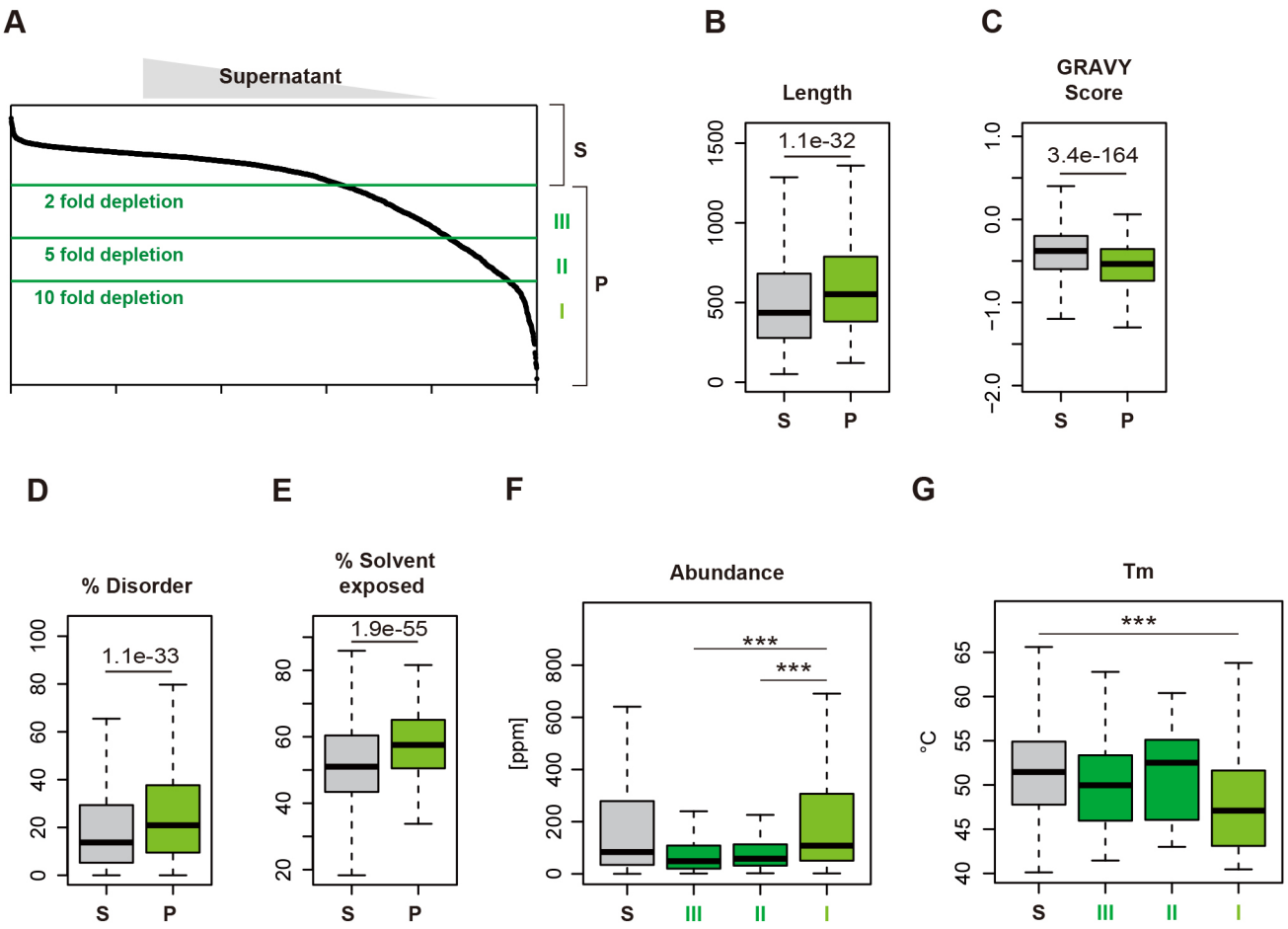

Fig. 2. Protein feature analysis of pelletable proteins upon heat shock. (A) Binning of data using two-, five- and ten-fold depletion from the supernatant as cutoffs to separate the data into soluble (S) and three pelletable (P) protein bins (I, II, III). (B–E) Box plots comparing distributions of soluble (S) and pelletable (P) proteins. The $\log_2$(H/L) in the proteomic analysis of the supernatant fraction was >−1 and <−1 for soluble and pelletable proteins, respectively. The following analyses are shown for sequence length in number of amino acids (B), hydrophobicity based on GRAVY score (C), percentage disordered residues (D) and percentage solvent exposed residues (E). *P*-values are shown. (F,G) Box plots comparing distributions of proteins in designated bins (as described in A) for protein abundance expressed in parts per million (ppm) (F) and T_m (°C) (G). ***$P \leq 0.001$. Horizontal bar indicates the median, the box shows the upper and lower quartiles, and whiskers show the range. All *n* and *P*-values are reported in Table S4.

Heat-induced pelletable proteins are enriched for stress granule localized proteins

Given the GO enrichment for SG localization among proteins that were mostly depleted from the supernatant after heat shock, we used confocal microscopy to determine which proteins colocalized with the poly-A binding protein and SG marker Pab1. Specifically, we assessed the 136 strains that were available from the yeast GFP collection for which the proteins were found depleted over tenfold from the supernatant (excluding membrane proteins). Following mating with a strain containing Pab1–mCherry, microscopy analysis identified 86 GFP-tagged proteins with a Pearson correlation coefficient (PCC) for colocalization with Pab1 larger than 0.2 after heat shock (Fig. 3A; Table S5). Notably, a drop in the PCC was observed below the 0.2 cutoff, and manual validation of microscopy images confirmed that no colocalization with Pab1 could be observed in these cells (Table S5). Typically, proteins with high (>0.45) and mid-range (<0.45 and >0.2) PCC displayed either full or partial colocalization with Pab1, respectively (Fig. 3B,C; Table S5). Importantly, none of these GFP tagged proteins form foci in unstressed cells (Koh et al., 2015). To assess the effect of the fluorescence tag on possible partial colocalization with Pab1, the GFP and mCherry tags were switched on a subset of these proposed heat SG components. In contrast to previous analysis, three tested proteins tagged to mCherry showed a full colocalization with Pab1–GFP after heat shock (Fig. S3A). Differences in the results (partial versus full colocalization of the assessed proteins with Pab1) can be attributed to the different tagging or marginal variations in the methods used to assess colocalization. Notably, a longer delay between the heat shock and cell imaging was introduced when assessing Pab1–mCherry colocalization due to technical limitations. Consistent with our previous analysis, heat-induced SG proteins have a lower apparent T_m (Fig. 3D). Interestingly, SG proteins with a higher PCC for Pab1 colocalization displayed slightly lower apparent T_m (difference not significant). Moreover, SG proteins with a high PCC were more often found to be associated with RNA (Fig. 3E). Of note, having a lower T_m is not characteristic of RNA-binding proteins, as analysis of all RNA-binding proteins did not display lower apparent T_m values (Fig. 3D). Moreover, SG proteins with a high PCC value have a significantly greater number of identified phosphorylation sites among known phosphorylated proteins (Fig. S3B). These results suggest that phosphorylation might play an important role in the regulation of SGs, as previously indicated (Kedersha et al., 1999; Reineke et al., 2017, 2012; Yoon et al., 2010). Low complexity regions (LCRs) have been implicated

Journal of Cell Science (2020) 133, jcs244657. doi:10.1242/jcs.244657

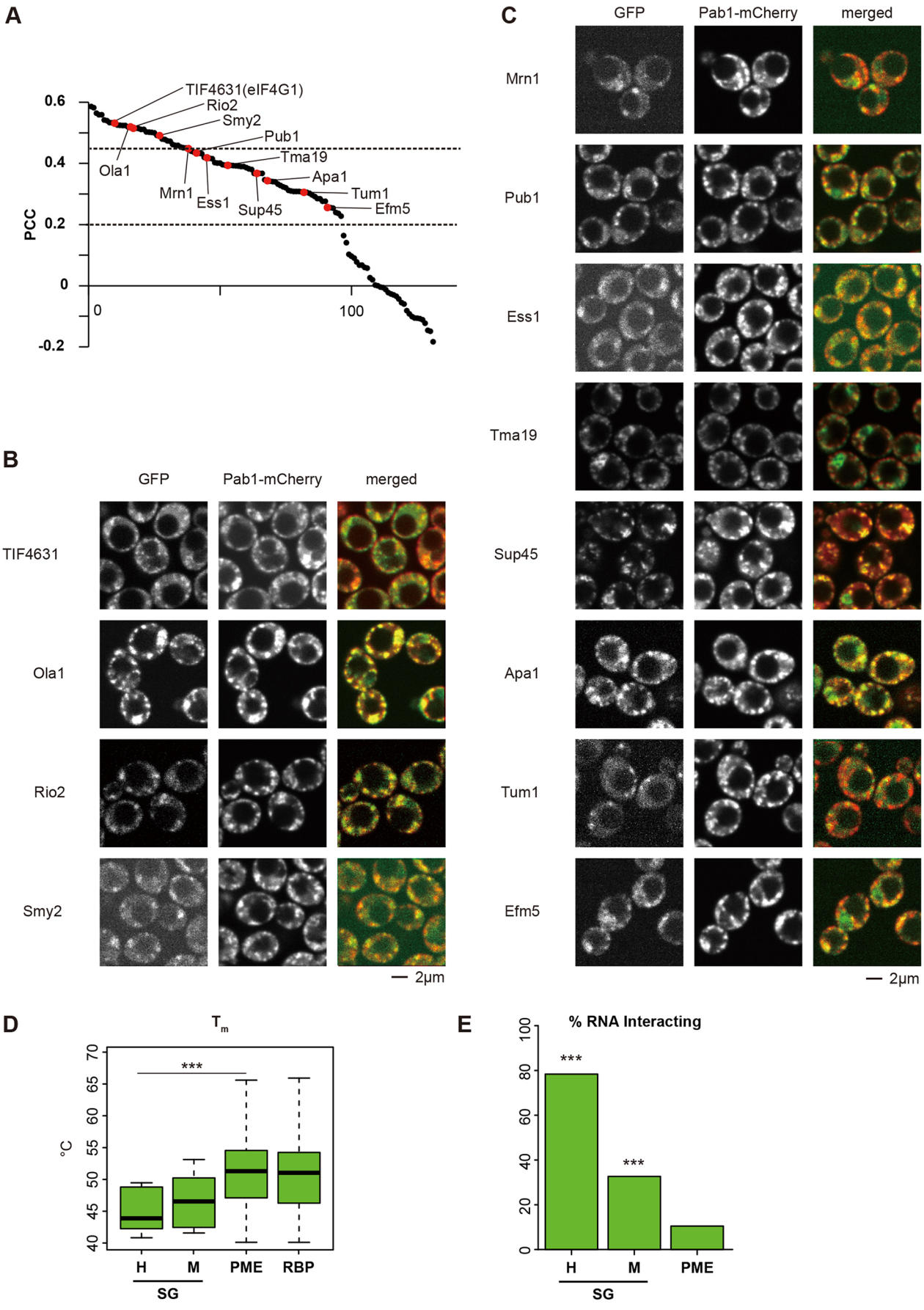

Fig. 3. See next page for legend.

Fig. 3. Colocalization analysis with stress granule marker Pab1. (A) Pearson correlation coefficient (PCC) of the colocalization between Pab1–mCherry and 136 GFP-tagged proteins, as assessed by confocal microscopy in diploid cells, ranked in descending order. Red dots highlight proteins shown in panels B,C. Dashed lines are thresholds that separate high, mid-range and non-colocalizing PCCs. (B,C) Representative images of quantified cells expressing Pab1–mCherry and selected GFP-tagged proteins (highlighted in A) with high (B) or mid-range PCC (C) values. (D) Box plot of the distributions of the apparent T_m among SG proteins with high PCC values (H; n=15) and mid-range PCC values (M; n=9), the proteome (PME; n=706), and all RNA-binding proteins in the proteome (RBP, n=244). Horizontal bar indicates the median, the box shows interquartile range (IQR), and upper whisker shows Q3 + 1.5 IQR and lower whisker shows Q1 − 1.5 IQR. (E) Bar plot shows whether or not SG proteins with high (H) or mid-range PCC (M) were found to bind RNA, compared to the proteome (PME). ***$P \leq 0.001$. All n and P-values are reported in Table S4.

in LLPS (Mitrea and Kriwacki, 2016; Molliex et al., 2015). We found that proteins that colocalize with Pab1 have a significant enrichment for LCRs with specific amino acids, especially for SG proteins with a high PCC (Fig. S3C). To summarize, we confirmed that a large proportion of the proteins depleted from the supernatant are recruited into heat-induced Pab1-containing granules, and identified 32 novel SG proteins that were not identified as such in previous studies (Cherkasov et al., 2015; Wallace et al., 2015).

Proteins in yeast heat stress granules are largely immobile

Yeast SGs have been previously shown to display a solid-like behavior, contrasting the liquid-like SGs found in mammalian cells (Kroschwald et al., 2015). However, the internal dynamics of individual yeast SGs in live cells remain unclear. To address this specific question, we measured the mobility of several SG proteins using FRAP. We selected the SG marker Pab1, the ATPase Ola1, which has been implicated in read-through of premature stop codons (high PCC in Fig. 3A), and the diadenosine phosphorylase Apa1 (mid-range PCC). After 10 min of heat shock at 45°C, the Pab1 signal in the photobleached foci recovered to ∼30% of its initial signal intensity, whereas the fluorescent signal of foci which were not photobleached decreased by ∼20% (Fig. 4A). The recovery of Pab1 was reduced to 21–22% following 15- and 20-min heat shock treatments. Noticeably, despite partial recovery of Pab1 signal in the photobleached area, no distinct inclusion sites were observed to have recovered. Interestingly, when FRAP was performed before the formation of distinguishable Pab1 foci (after a 5 min heat shock at 45°C), the cytosolic region revealed decreased mobility (Fig. S4A). As a control, we selected a protein that remained soluble after heat shock based on our mass spectrometry data, Tpi1, and observed that Tpi1–GFP did not form foci after 15 min of heat shock at 45°C (Fig. S4B). Importantly, the fluorescence signal in the photobleached area of heat shocked Tpi1–GFP cells showed a fast recovery, below the 5 s time frame required for image acquisition (Fig. S4B). These results indicate that, whereas a small fraction of Pab1 may remain dynamic in the cell or dissociate from the SG, most remains associated with the foci. These results are similar to what was observed in Pab1 droplets assembled *in vitro* (Riback et al., 2017). Additionally, Ola1 showed a minimal recovery (Fig. 4B) after forming detectable foci after 5 min of heat shock at 45°C. An ∼15% recovery of signal intensity was observed 90 s post-photobleaching. Longer periods of stress prior to photobleaching (10- and 15-min heat shock) led to a further decreased recovery of 4–7% of the initial signal intensity. Remarkably, Apa1 did not appear to be dynamic after heat shock despite displaying a lower PCC with Pab1 (Fig. 4C). Apa1 showed a 9–10% recovery after 10- and 15-min heat shock at 45°C. These results confirm that components of yeast heat SGs display poor protein dynamics once recruited to these heat-induced compartments.

Intrinsically disordered regions can be sufficient for stress granule recruitment

Our finding that proteins with reduced solubility after heat stress are enriched in IDRs and localize to SGs is consistent with the observation that RNP proteins often contain IDRs (Decker et al., 2007; Hennig et al., 2015; Jain et al., 2016; Protter et al., 2018). However, to our knowledge, the enrichment of IDRs within yeast SGs has not been clearly established and characterized. Therefore, we sought to evaluate whether IDRs are necessary or sufficient for proteins to coalesce into heat SGs. It has been shown that a short, disordered segment of low sequence complexity is responsible for the recruitment of Cdc19 to starvation-induced granules and this short peptide is sufficient to drive GFP into granules (Saad et al., 2017). We used a similar approach and expressed GFP-tagged IDRs of 11 SG proteins from a plasmid. Five of the 14 IDRs that we assessed were able to drive GFP localization into Pab1 foci after heat shock while the signal remained diffuse in untreated cells (Fig. 5A; Fig. S5A,B). IDRs of Ubp3, Psp2, Dcp2, and Tif4631 (also known as eIF4G1) showed strong recruitment to foci, whereas the IDR of Mot2 led to a weaker but distinct GFP signal in Pab1 foci. IDRs of Ubp3, Dcp2, Mot2, and Tif4631 contain one or more patches with predicted aggregation-prone sequence or with an enhanced score for prion-like amino acid composition (Fig. 5A). In addition, all five IDRs contain regions with low complexity amino acid sequences. However, those LCRs lack a consensus in amino acid enrichment. Ubp3, Psp2, and Dcp2 IDRs share LCRs enriched with asparagine, whereas the Mot2 and Tif4631 SG-incorporated IDRs lack this feature. Furthermore, asparagine LCRs are also found in three of the non-SG recruited IDRs (Smy2, Caf40 and the N-terminal Tif4631 IDR; Fig. S5C). Histidine LCRs did uniquely appear in those IDRs that are recruited into SGs; however, this region only appeared in Ubp3. Additionally, all five IDRs contain molecular recognition features (MoRFs), which are short segments in IDRs that adopt secondary structures upon binding to other domains. Nonetheless, IDRs that failed to be recruited to SGs also contain similar features (Fig. S5C). Thus, none of these features may be sufficient, when examined individually and in the general case, to explain IDR SG incorporation. Next, we sought to determine whether these five IDRs could also be recruited to SGs induced by other stresses. Excluding the IDR (829–952) of Tif4631, these IDRs were also recruited into Pab1-containing granules under glucose starvation (Fig. 5B; Fig. S5D). Similarly, the IDR of Ubp3 and Psp2 were distinctively recruited to Pab1 foci upon azide treatment (Fig. 5C), whereas recruitment of the IDRs of Mot2 and Dcp2 appeared more modest. Importantly, these results show that several IDRs could be directly recruited into SGs, in contrast to a recent report in which none of the assessed IDRs was sufficient to target components to RNP granules (Protter et al., 2018).

Associations between IDRs and SG compartments display different properties

Ubp3 is a deubiquitinase and was recently shown to be important for the assembly of SGs upon glucose starvation and heat shock (Nostramo et al., 2016). Ubp3 was also shown to be involved in Rsp5-dependent proteasomal degradation of misfolded proteins upon heat shock (Fang et al., 2016). Psp2 is an asparagine-rich RNA-binding protein that was recently shown to promote the formation of P-bodies in some conditions (Rao and Parker, 2017). The IDR of Psp2 contains several RGG motifs in its IDR, which

Journal of Cell Science (2020) 133, jcs244657. doi:10.1242/jcs.244657

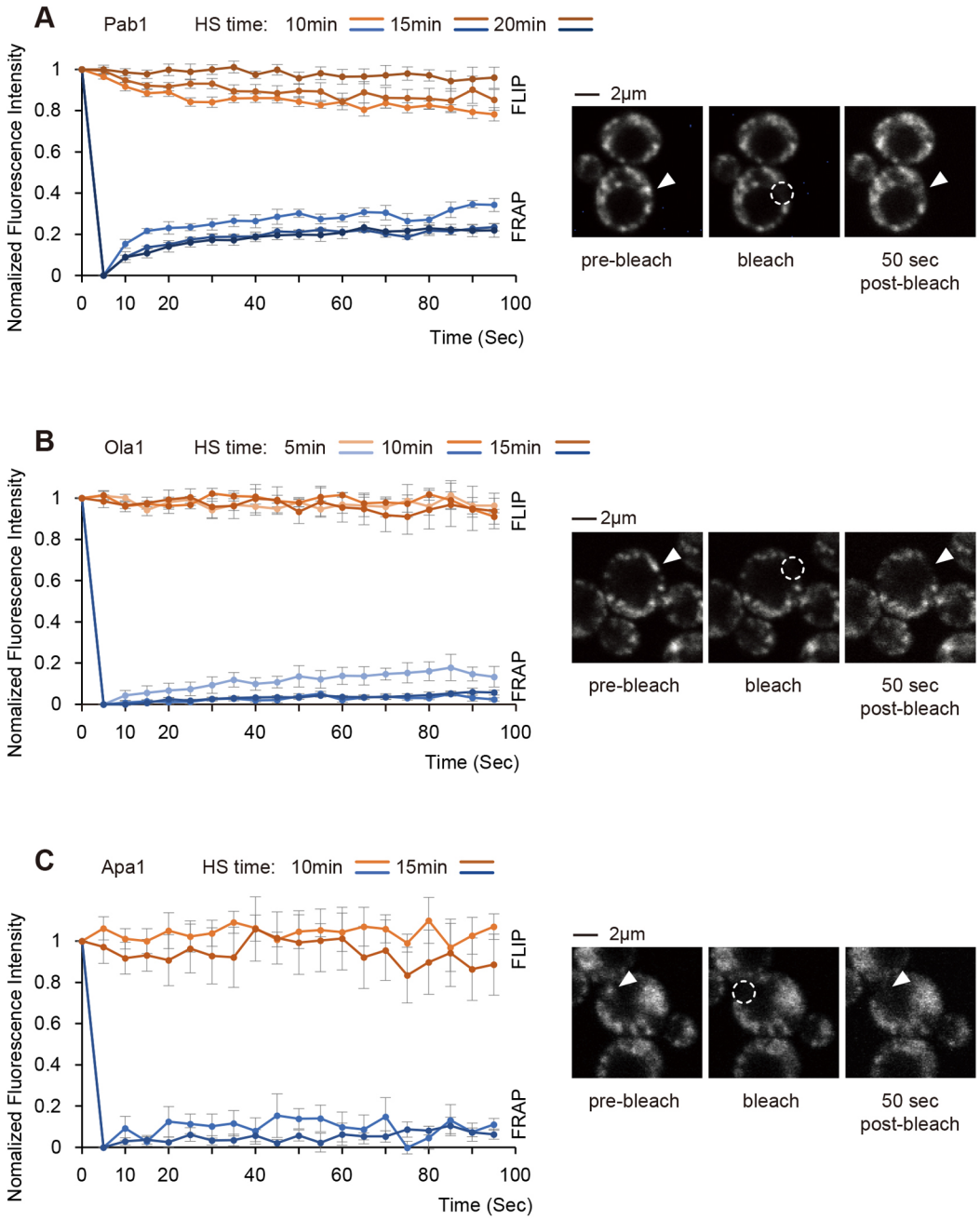

Fig. 4. Components of heat-induced stress granules are poorly mobile. (A–C) FRAP and fluorescence loss in photobleaching (FLIP) of Pab1 (A), Ola1 (B) and Apa1 (C) tagged with GFP at their endogenous locus. The graphs show the averaged signal intensities from six replicates (mean±s.e.m.) at the indicated time points after incubating the cells at 45°C for the indicated time periods (HS time). FLIP data was measured in three regions of interest (ROI) containing unbleached foci within a bleached cell. Representative cells are shown on the right. The dotted circles represent the photobleached ROIs and the arrowheads indicate the analyzed foci before and 50 s after photobleaching.

have previously been implicated in protein LLPS (Chong et al., 2018). Interestingly, whereas the IDR of Ubp3 remained in the pellet fraction after centrifugation, the IDR of Psp2 was largely in the supernatant after heat shock (Fig. 6A). These findings suggest that the association of the IDR of Psp2 with the SG is potentially more transient allowing for rapid exchange between the pellet and supernatant fractions. To test this hypothesis, FRAP was employed to compare the mobility of both IDRs. As expected, we found that the IDR of Ubp3 displayed minor recovery, similar to Ola1, Apa1 and full-length Ubp3 (Fig. 6B). In contrast, the IDR of Psp2 was found to be rapidly recruited to the foci within 5 s after photobleaching, with a signal recovery of ∼80% of the initial intensity (Fig. 6B). This dynamic recovery was limited to the IDR of Psp2, as the full-length Psp2 only showed modest resurgence. These results suggest that the IDRs of Ubp3 and Psp2 associate with SGs using different mechanisms. To determine whether these interactions are intra- or inter-molecular, we next assessed the ability of these IDRs to be recruited into foci in the absence of the respective full-length proteins. The IDR of Ubp3, but not that of Psp2, coalesced in *ubp3*Δ and *psp2*Δ cells, respectively (Fig. 6C), suggesting that the IDR of Ubp3 might be recruited to the heat SGs by binding to another protein. In contrast, the IDR of Psp2 requires

Journal of Cell Science (2020) 133, jcs244657. doi:10.1242/jcs.244657

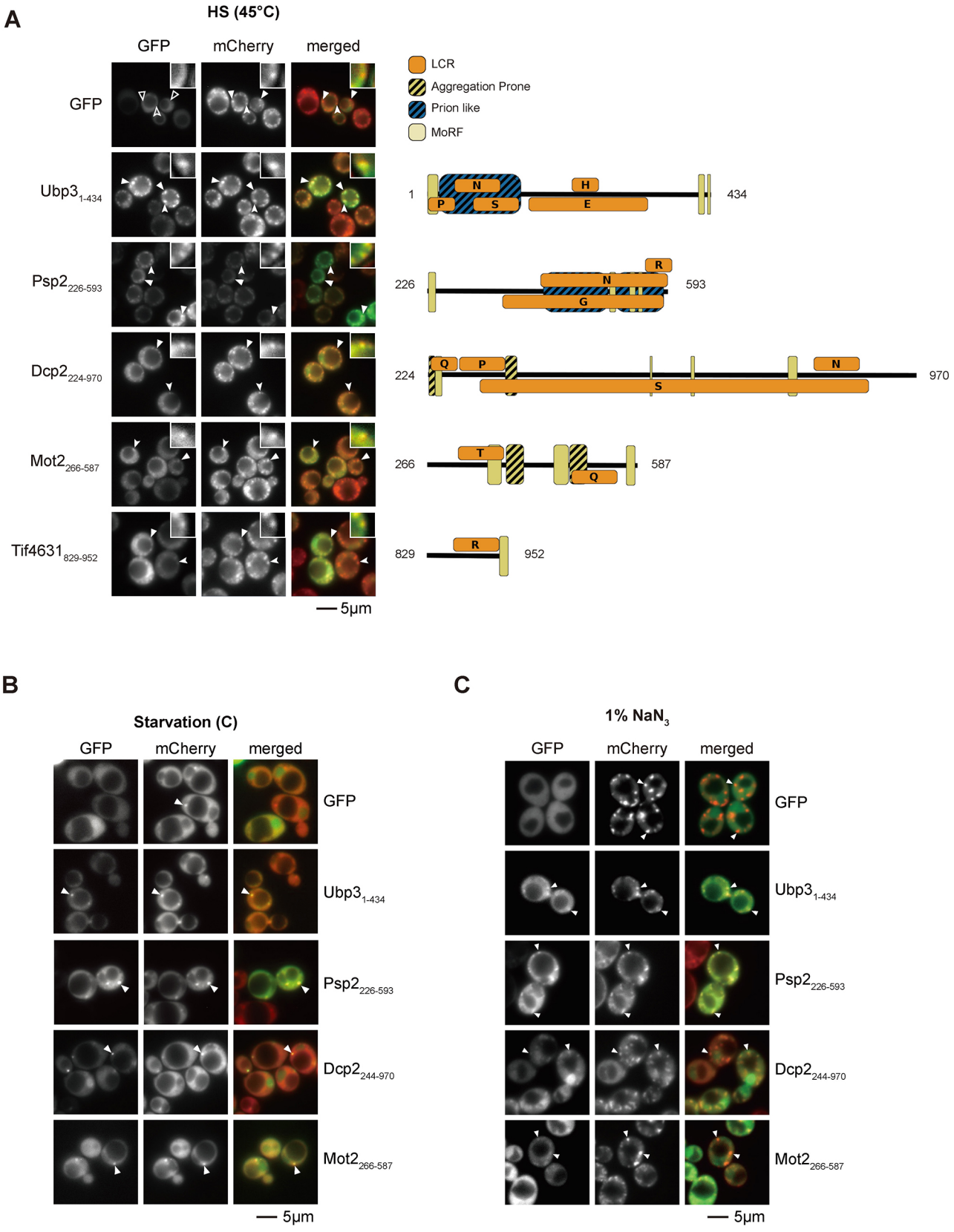

Fig. 5. See next page for legend.

the presence of full-length Psp2 for SG localization, indicating that the IDR likely interacts with the N-terminal region of Psp2. Indeed, the structured region of Psp2 (residues 1–225), which has one RNA recognition motif, was recruited into Pab1 foci independently of the IDR (Fig. S6A). These results show that IDRs associate to SGs in different manners, and the IDR of Psp2 appears to be more dynamic.

Journal of Cell Science (2020) 133, jcs244657. doi:10.1242/jcs.244657

Fig. 5. Recruitment into stress granules by intrinsic disordered regions. (A) Representative images of Pab1–mCherry cells that expressed from a plasmid the designated disordered regions tagged with GFP. Cells were exposed to a 15 min heat shock at 45°C prior to imaging. Filled arrowheads designate representative Pab1 and GFP foci. Open arrowheads show lack of foci fomation in the GFP channel. The insets show a five-times magnified image of the foci designated by a sunken arrowhead. Feature analysis of the corresponding IDR is shown on the right. Orange boxes indicate low complexity regions, with letters to indicate specific amino acid enrichment, black striped boxes indicate predicted aggregation prone regions, blue striped boxes indicate prion-like composition, and yellow boxes indicate predicted MoRFs. Only highly significant ($P \leq 1 \times 10^{-6}$) low complexity regions are pictured. (B,C) Same as in A, but upon carbon starvation for 90 min (B) or after 30 min incubation at 30°C with 1% NaN_3 C. Exposure time for GFP was increased in C due to dimmer signal in these conditions.

Furthermore, these results indicate that the yeast heat-induced compartments are not static macro-assemblies with limited diffusion, because some of their components can freely associate and dissociate following their formation.

The IDR of Ubp3 is required for its role in stress response

We next wanted to assess whether the IDR of Ubp3 was vital for SG formation. Although we were not able to observe a clear decrease of SG formation in *ubp3*Δ cells by monitoring Pab1-foci under heat shock conditions (Fig. S6B), lack of Ubp3 led to the absence of Pab1 foci in azide-treated cells (Fig. 6D), as previously reported (Nostramo et al., 2016). Importantly, expression of a truncated Ubp3 that lacks the IDR could not rescue SG formation (Fig. 6D). Intriguingly, the loss of Ubp3 function also led to a marked increase of cells that do not display a single, large vacuole after heat shock (Fig. S6B). Accordingly, the expression of wild-type Ubp3 abrogated this phenotype in *ubp3*Δ cells, whereas expression of the Ubp3 IDR alone led to a partial rescue and expression of the truncated Ubp3 that lacked the IDR only provided a mild rescue (Fig. S6B). These results highlight how the presence of the Ubp3 IDR plays a role in the stress response and the assembly of SGs under specific stresses, possibly by recruiting substrates and the Bre5 cofactor, which forms a complex with Ubp3 by interacting with the Bre5-binding domain within the IDR of Ubp3 and is required for the activity of the deubiquitinase (Li et al., 2007, 2005).

DISCUSSION

In this study, we employed a proteomic approach to assess how heat shock alters protein sedimentation and show that heat-induced pelletable proteins share common characteristics. Combining proteomic results with high-content imaging, we identify 32 novel heat SG-localizing proteins. We further confirm that several components of yeast heat SGs are highly static and that IDRs are able to drive SG recruitment.

Although the focus of this study centered on the recruitment of proteins into cytosolic heat SGs, several proteins depleted from the supernatant fraction after heat shock did not localize to Pab1-containing inclusions. These include proteins from mitochondria, the nucleus and nucleolus, similar to what was observed previously (Cherkasov et al., 2015). Interestingly, almost all of the proteins that were lost in heat shocked cells in the low centrifugation pre-clearing step prior to fractionation are known to be localized to the nucleus or nucleolus, and more than one-third of those proteins are involved in assembly of the pre-90 S ribosome. Because nucleolus proteins phase separately during ribosome assembly (Mitrea et al., 2018), it is possible that these macro-assemblies in the nucleolus undergo additional rearrangements upon heat shock leading to a higher density compartmentalization. We found that mitochondrial proteins also form foci after heat shock that do not colocalize with Pab1 (Table S5). Thus, mitochondria, or some elements of this organelle, might also undergo a drastic rearrangement during acute heat stress.

Previous work from Drummond and colleagues indicates that protein coalescence after heat shock is a reversible process that does not rely on proteolysis to 'regenerate' the bulk of soluble proteins after the stress recovery (Wallace et al., 2015). We found that the proteins that were most depleted from the supernatant (group I) are also highly abundant. This observation is consistent with the work from Drummond and colleagues, as the degradation of abundant proteins upon stress recovery would present a clear evolutionary disadvantage. The fact that these abundant proteins were mostly depleted from the supernatant fraction (>90%) also indicates that the compartmentalization of these proteins is highly efficient. Recent proteomic studies using proximity tagging show that many SG components interact in unstressed and stressed cells (Markmiller et al., 2018; Youn et al., 2018). These studies indicate that the process is likely tightly regulated in order to only drive coalescence after the stress. The prevalence of charged residues and potential phosphorylation sites among pelletable and SG proteins supports a role for electrostatic interactions in stress-induced condensates that may be, in part, regulated by kinases. Importantly, we confirmed these results in a recent meta-analysis that includes yeast and human SG proteins from other studies (Kuechler et al., 2020).

SGs that assemble upon acute heat shock in yeast have been shown to harbor misfolded proteins (Cherkasov et al., 2013; Mateju et al., 2017). The lower apparent melting temperature of SG proteins suggests that many SG proteins undergo a structural transition during heat shock. Such a change would allow for the exposure of buried, hydrophobic residues for additional promiscuous interactions that would increase protein valency, thus aiding the demixing process of heat SG components (Li et al., 2012). It should be noted that the apparent T_m measurements derived from the proteomic analysis were done at the peptide level, and that the measured values were not always equivalent across a given polypeptide (especially in multi-domain proteins) (Leuenberger et al., 2017). Therefore, misfolding of highly pelletable proteins could be partial (i.e. specific to a domain within a polypeptide) to potentially retain functionality of the protein, as shown previously (Wallace et al., 2015), and to facilitate recovery. In addition to proteins that are predominantly depleted from the supernatant after heat shock, a sizable proportion of the proteome was also affected, but to a lesser extent (designated groups II and III in Fig. 2). Examination of a few of these proteins showed that they were weakly recruited to foci (for example, YLR287c and Dph6 in Fig. S1C). One possibility is that many of these proteins misfold, leading to their SG recruitment. Under a prolonged heat shock, their SG recruitment could be enhanced due to more exposed misfolded regions. Interestingly, these proteins are of lower abundance in the cell, consistent with a possible lower selective pressure to maintain them in a folded state upon acute stress. Future investigations should determine whether newly synthesized proteins are more susceptible to misfolding and SG recruitment.

We found that there is an enrichment of IDRs among the heat-induced pelletable proteins. We have confirmed that IDRs are enriched in yeast SGs in a meta-analysis that we carried out alongside this study (Kuechler et al., 2020). Many studies have investigated the role of IDRs, particularly prion-like domains and IDRs with low complexity, in protein phase separation or RNP granule formation (Decker et al., 2007; Gilks et al., 2004; Kato et al., 2012; Protter et al., 2018). In particular, Protter et al. (2018) tested

Journal of Cell Science (2020) 133, jcs244657. doi:10.1242/jcs.244657

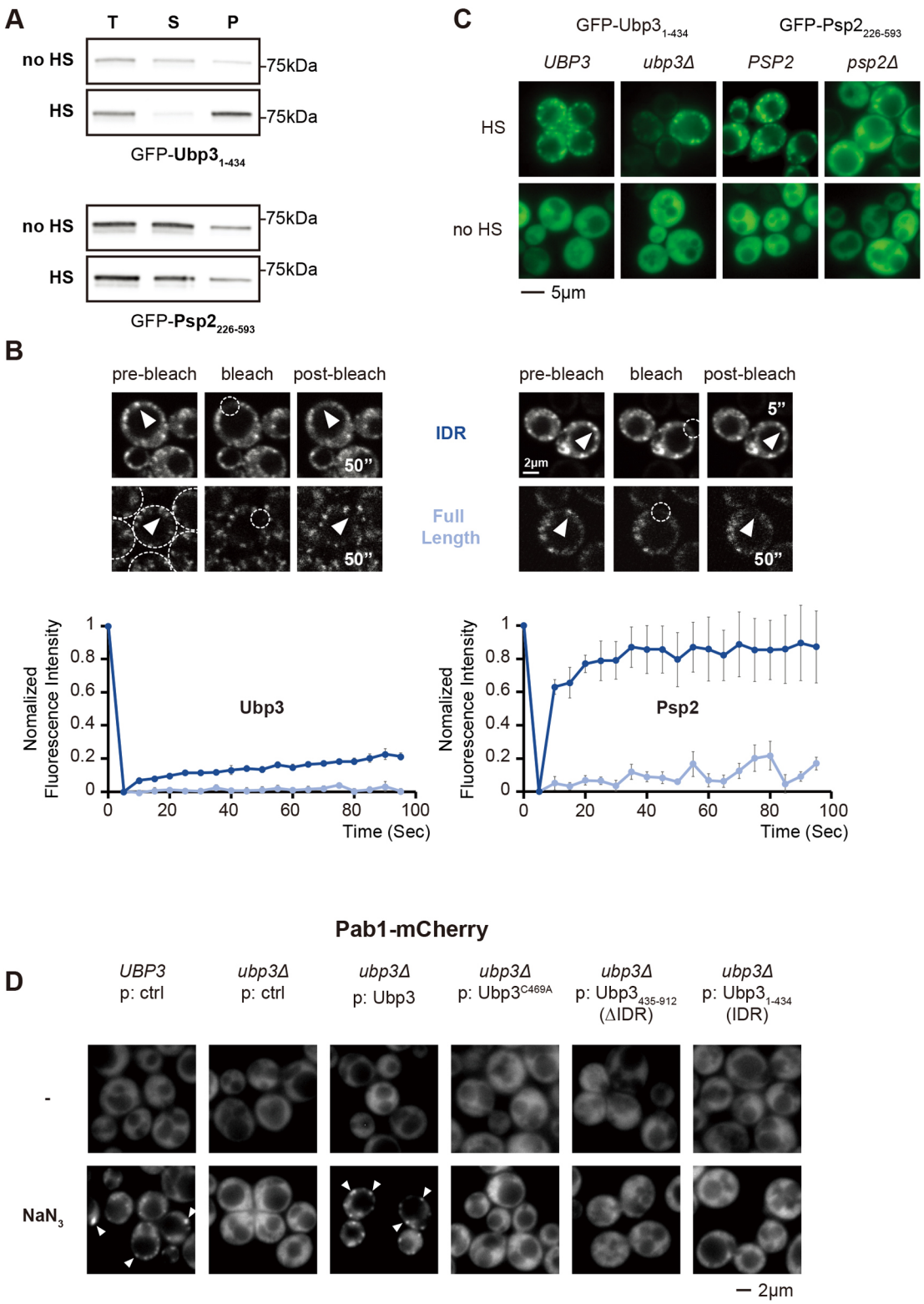

Fig. 6. IDRs from Ubp3 and Psp2 display different properties. (A) Western blot against GFP in the indicated lysate fractions derived from unstressed (no HS) and heat shocked (HS) cells expressing the indicated GFP-tagged IDRs. T, total cell lysate; S, supernatant; P, pellet. (B) FRAP in heat shocked cells (15 min at 45°C) expressing the designated disordered regions (dark blue) or full-length proteins (light blue) tagged with GFP. The IDR segments fused to GFP were expressed from a plasmid, whereas the full-length proteins were endogenously tagged. Representative cells are shown on the top. The dotted circles represent the photobleached ROIs and the arrowheads indicate the analyzed foci before and 50 s or 5 s after photobleaching. The graphs show the averaged signal intensities from six cells quantified sequentially (mean±s.e.m.) at the indicated time points. (C) Representative images of the indicated wild-type or mutant cells expressing from a plasmid the designated disordered regions tagged with GFP, before and after heat shock. (D) Representative images of Pab1–mCherry cells with the indicated genetic background and protein expressed from a plasmid (p) before (–) and after 30 min incubation at 30°C with 1% NaN_3. Arrowheads designate representative Pab1 foci. No Pab1 inclusion was observed in the absence of wild-type Ubp3 in three independent experiments.

IDRs from four yeast P-body proteins and found them neither sufficient nor necessary for P-body targeting. In contrast, we found at least five IDRs that are sufficient to mediate SG recruitment of the fused GFP moiety. Interestingly, we characterized IDRs of two proteins that also localize to P-bodies (Psp2 and Dcp2). Although these IDRs form foci under stress conditions, we did not observe any obvious foci in unstressed conditions, in which P-bodies are also present. One possibility is that distinct elements might mediate recruitment of these proteins to different RNP granules. All five IDRs contain distinct protein sequence features that might contribute to their ability for SG recruitment but none that are universal or unique. Perhaps the presence of longer prion-like domains in the IDRs of Psp2 and Ubp3 contribute to a higher likelihood of LLPS, and thus to SG incorporation. All of the tested IDRs contain several compositionally biased regions of low complexity; however, due to the relatively small group of IDRs assessed, it remains difficult to conclusively link any of these features to SG recruitment with confidence. Moreover, we speculate that it is likely that SG incorporation is either controlled through direct interactions or through the fine tuning of protein solvation behavior which, by necessity, is specific to each protein. Therefore, IDRs recruited to SGs might not share a singular common feature. Nonetheless, the analysis of the diffuse behavior of Ubp3 and Psp2 in SGs revealed that IDRs located to SGs can display pronounced differences in dynamics, which is presumably reflective of their respective affinity for other domains within these membraneless compartments. Because the structured regions of both Ubp3 and Psp2 proteins were also recruited to Pab1 foci (Fig. S6A), their IDRs might further facilitate recruitment to SGs by adding valency, increase the affinity for partners within the stress compartment, and/or alter the solvation properties of the proteins. In the case of Ubp3, the IDR plays a role in SG assembly. In some cases, the presence of an IDR is a predominant feature for SG proteins but their affinity to other SG components alone may be too weak for incorporation. Alternatively, they could also facilitate recovery after stress, similar to what has recently been shown for the Sup35 prion-like domain (Franzmann et al., 2018).

MATERIALS AND METHODS

Yeast strains and plasmids

For SILAC, a modified BY4741 *Saccharomyces cerevisiae* yeast strain was used (YTM1173, *MATa*, *his3Δ1*, *leu2Δ0*, *ura3Δ0*, *MET15*, *arg4Δ::KanMX6*, *lys2Δ0*). The Pab1–mCherry strain (YTM1920; *MATα*, *his3Δ1*, *leu2Δ0*, *lys2Δ0*, *ura3Δ0*, *Pab1-mCherry::KanMX6*) was generated by homologous recombination using a yeast codon-optimized mCherry placed into pFA6a-kanMX6 (BPM866). *TMA1*, *ESS1* and *MRN1* were similarly modified from the BY4742 strain. Cells with mCherry-tagged alleles were then mated with selected strains from the yeast GFP collection (Huh et al., 2003, gifts from Dr Phil Hieter, Michael Smith Laboratories, The University of British Columbia, Canada) to generate diploid cells for colocalization analysis. For the analysis of IDRs, as well as Ubp3 and its mutants, the indicated gene segments were amplified from yeast genomic DNA and subcloned C-terminally of GFP using EcoRI/NotI and SalI restriction sites, into a modified pRS313 with the GPD promoter and *PGK1* terminator sequences (BPM1174–1220, 1453–1454).

Yeast culture and sample preparation

Yeast cells were incubated at 25°C, unless otherwise stated. For SILAC, cells were grown in light-labeled (0.03 mg/ml Lys-0, 0.02 mg/ml Arg-0) or heavy-labeled (0.03 mg/ml Lys-4, 0.02 mg/ml Arg-6) amino acid (Lys-4: Cambridge DLM-2640-PK; Arg-6: Cambridge CLM-2265-H-PK) in synthetic defined medium (Cold Spring Harb Protoc 2015. doi:10.1101/pdb.rec085639) with 2% dextrose for at least 7 generations. Heat shock was performed in a shaking water bath at 45°C for 20 min before harvest. Equal OD_{600} of light- and heavy-labeled cells were collected at mid-log phase (OD_{600}=0.8–1) by centrifugation at 3220 ***g*** for 5 min at 4°C, washed twice with cold 1×TBS (50 mM Tris-HCl pH 7.5, 150 mM NaCl), mixed, and resuspended in equal volume of 2×native lysis buffer [200 mM Tris-HCl pH 7.5, 150 mM NaCl, 2 mM PMSF, 2×protease inhibitor cocktail (Sigma-Aldrich) and 2 mM 1,10-phenanthroline]. Resuspended cells were snap-frozen drop by drop in liquid nitrogen. The resulting cell pellets were lysed by cyro-grinding in liquid nitrogen with a mortar and pestle mounted on an electric driver (OPS Diagnostics). The lysate was thawed on ice and further diluted three times by adding ice-cold 1×native lysis buffer and 1% NP40 (final concentration). Total cell lysate was pre-cleared twice by centrifugation at 1000 ***g*** at 4°C for 15 min. The pellet fraction was separated by centrifugation at 16,100 ***g*** at 4°C for 15 min. The insoluble protein pellet was washed twice with ice-cold 1×native lysis buffer containing 1% NP40 and re-solubilized in 1×Laemmli sample buffer (62.5 mM Tris-HCl pH 6.8, 2% SDS and 10% glycerol). Protein concentrations were determined by using a BioRad DC™ protein assay. Three biological replicates were produced to ensure data reproducibility.

Mass spectrometry

200 µg of protein samples from pellet, supernatant or total cell lysate fractions were in-gel trypsin digested, as previously described (Shevchenko et al., 1996). The resulting peptides were desalted with high-capacity C18 (Phenomenex) STAGE tips before an offline high pH reversed-phase chromatography fractionation, as previously described (Udeshi et al., 2013). Fractions were collected at 2 min intervals. The resulting fractions were pooled in a non-contiguous manner into eight fractions for each SILAC experiment. Each fraction was then dried in a Vacufuge Plus (Eppendorf).

Mass spectra were acquired on an Impact II (Bruker) on-line coupled to either an EASY-nLC 1000 (Thermo Scientific) or a nanoElute (Bruker) liquid chromatography system (LC). The LC was equipped with a 2-cm-long, 100-µm-inner diameter trap column packed with 5 µm-diameter Aqua C-18 beads (Phenomenex) and a 40-cm-long, 50-µm-inner diameter fused silica analytical column packed with 1.9 µm-diameter Reprosil-Pur C-18-AQ beads (Dr Maisch). Samples were run with a 120 min gradient from 10% Buffer B (0.1% formic acid and 80% acetonitrile in water) to 17% Buffer B during the first 45 min, then Buffer B was increased to 35% by 90 min and to 80% at 95 min. The scanning range was from *m*/*z* 200 Th to *m*/*z* 2000 Th. The data-dependent auto-tandem mass spectrometry (MS/MS) mode was set to fragment the 17 most abundant ions with an exclusion window of 0.4 min.

All raw proteomics data have been deposited to the ProteomeXchange Consortium through the PRIDE partner repository with the identifier PXD012631 (Deutsch et al., 2017; Vizcaíno et al., 2014). The results were analyzed against SGD_orf_trans_all_20110203 released from the *Saccharomyces* Genome Database (https://www.yeastgenome.org/) with common contaminants using the latest version of MaxQuant software when the data was generated (version 1.5.2.8). The searches were done using the default software settings, plus match-between-runs and re-quantification and an FDR set below 0.01.

Bioinformatics

The median $\log_2$ ratio of total cell lysate was calculated and subtracted from all supernatant ratios to correct for error in mixing. Samples were then binned according to loss of solubility upon heat shock, or PCC score.

All figures were generated using the R package (R Core Team, 2018) and assembled using Adobe Illustrator. Computational analysis was carried out using in-house Perl scripts and statistical tests were performed in R. In all cases of non-binary data, *P*-values were obtained using the Mann–Whitney–Wilcoxon test in conjunction with the Benjamini–Hochberg procedure for multiple testing correction to determine significance thresholds and reduce the false discovery rate (Bauer, 1972). In the case of binary data, the data was scrutinized against a hypergeometric distribution to determine significance. The significance threshold for data was set at a *P*-value less than or equal to 0.05.

IDRs were determined with DISOPRED3 (Jones and Cozzetto, 2015). Patches of disordered amino acids were identified using a sliding window of 30 amino acids, which allowed for up to five amino acids to be considered as 'not disordered' before truncating the disordered stretch. Protein abundances were taken from the integrated yeast proteome data in PaxDb

4.0 (Wang et al., 2015). Solvent exposure calculations were performed using the SSpro8 and ACCpro software in the SCRATCH-1D 1.1 package (Magnan and Baldi, 2014). GRAVY score was calculated with in-house scripts using previously derived parameters (Kyte and Doolittle, 1982). Motif identification was carried out using the Analysis of Motif Enrichment (AME) tool (McLeay and Bailey, 2010) in the MEME-Suite of software (Bailey et al., 2009) using the Fisher test criteria, the average scoring method, and a background of shuffled proteins of the yeast proteome. Low complexity regions were calculated using fLPS (Harrison, 2017) with default settings. Apparent T_m data was taken from the study performed by Leuenberger et al. (2017). RNA interacting proteins were identified from cross-linking studies by Beckmann et al. (2015), Phosphorylation data was obtained from dbPTM (Huang et al., 2016). Molecular recognition features (MoRFs) were identified using the MoRF CHiBi System (Malhis et al., 2015).

Aggregation-prone patches and prion-like composition were determined using TANGO (Linding et al., 2004) and PLAAC (Lancaster et al., 2014) software packages, respectively.

Microscopy

For epifluorescence microscopy, cells were grown to mid-log phase (~OD_{600}=0.6) in synthetic defined medium with low fluorescence yeast nitrogen base (LoFlo, Formedium) and 2% dextrose. 1 ml of cultures were heat shocked in a thermomixer at 45°C for 15 min. Cells were subsequently collected by centrifugation at 6000 ***g*** for 30 s. For starvation, cells were incubated in LoFlo medium without dextrose for 90 min before imaging. For azide treatment, cells grown at 25°C were treated with 1% NaN_3 (w/v) for 30 min at 30°C before imaging. Live cells were resuspended in growth medium before imaging with a Zeiss AxioObserver Z1 equipped with a 470 nm and 590 nm Colibri light source and a 63×1.4 NA oil immersion DIC objective. Images were acquired and processed using the Zen2 software (Carl Zeiss Microscopy GmbH).

The diploid strains with Pab1–mCherry and a candidate protein fused to GFP were inoculated into a 384-well glass-bottom optical plate (Greiner) using a pintool (FP1 pins, V&P Scientific) operated by a Tecan robot (Tecan Evo200 with MCA384 head) and grown at room temperature overnight. Upon reaching an OD_{600} equal to ~0.5 the plate was heated by a plate heater set to 48°C (Torrey Pines Scientific) for 20 min. Following the heat shock, imaging was performed using an automated Olympus microscope X83 coupled to a spinning disk confocal scanner (Yokogawa W1), using a 60× objective (Olympus, plan apo, 1.42 NA). All strains were imaged within a 15 min time period. Excitation was achieved with a green LED for brightfield images, a 488 nm laser (Toptica, 100 mW) for GFP, and a 561 nm laser (Obis, 75 mW) for mCherry. Emission filter sets used to acquire the brightfield, GFP and mCherry images were 520/28, 520/28 and 645/75, respectively. The same triple-band dichroic mirror was used for all channels (405/488/561, Yokogawa). Images were recorded on two Hamamatsu Flash4-V2 cameras, one for the brightfield and GFP channels and the second for the mCherry channel. Each image set was composed of two brightfield (BF) images (one in focus and one defocused to facilitate cell segmentation, each with 30 ms exposure) as well as one image for each fluorescent channel (500 ms exposure for GFP and 500 ms exposure for Pab1–mCherry). The focus was maintained throughout the experiment using hardware autofocus (Olympus *z*-drift compensation system).

To detect colocalization in individual cells, we first segmented cells using the brightfield image, as previously described, and referred to each cell as a region of interest (Matalon et al., 2018 preprint). To quantify subcellular colocalization within each cell, we selected pixels with fluorescence intensity above a brightness threshold (30th percentile) and calculated, based on those, the Pearson correlation coefficient (PCC) between green and red pixel intensities:

$$\mathrm{PCC} = \frac{\sum_i [(R_i - \bar{R}) \times (G_i - \bar{G})]}{\sqrt{\sum_i (R_i - \bar{R})^2 \times \sum_i (G_i - \bar{G})^2}},$$

where R_i and G_i refer to the intensity values of the pixels in the red and green channels, and $\bar{R}$ and $\bar{G}$ refer to the mean intensities of the red and green channels, respectively, across the entire cell. PCC values range from 1 for cells whose fluorescence intensities are completely linearly related, to −1 for cells whose fluorescence intensities are totally inversely related to one another. The median PCC calculated on a cell population (of typically 300 cells) was used to quantify the colocalization of a candidate protein with Pab1. All the scripting for image analyses was carried out using Fiji ImageJ (Schindelin et al., 2012).

FRAP

Images were acquired using an Olympus Fluoview FV1000 laser scanning confocal microscope with an UplanSApo 100×1.40 oil immersion objective. The selected region of interest (ROI) was photobleached with a 405 nm diode laser. Images were acquired every 5 s for 20 frames after the initial photobleach. For FRAP, the signal was monitored in the photobleached ROI. For fluorescence loss in photobleaching (FLIP), the signal of three additional ROIs that contained cytosolic foci was averaged. Three additional ROIs from adjacent cells that were not bleached were also monitored for photofading. Fluorescence of ROI was calculated by first removing background signal, then correcting for photofading and normalizing across replicates by standardization and feature scaling.

Western blotting

A 100 ml volume of cell culture was either directly collected at OD_{600}=0.8–1 or subjected to heat shock at 45°C for 20 min. Cells were washed twice with 1×native lysis buffer before resuspension in 100 µl of 1×native lysis buffer and lysis by glass beating. Cell debris was then removed by two 1000 ***g*** centrifugation steps for 5 min. 100 µl of total cell lysate was centrifuged at 16,100 ***g*** for 15 min. 25 µg of total cell lysate and equal corresponding volumes of supernatant and pellet fractions were resolved by SDS–PAGE using 4%–20% gradient gels for western blotting with anti-GFP antibodies (1:1500; Roche, catalog # 11814460001) and LI-COR secondary antibodies (1:10,000; IRDye® 800CW goat anti-mouse IgG secondary antibody; catalog # 926-32210). Images were captured and quantified using a CLx Odyssey system using Image Studio v3.1 (LI-COR Biosciences).

Acknowledgements

We thank Dr P. Hieter and Tejomayee Singh for sharing strains from the GFP Collection, Dr N. Stoynov for his help with mass spectrometry experiments, Dr G. Cohen Freue for advice and members of the Mayor laboratory for discussions.

Competing interests

The authors declare no competing or financial interests.

Author contributions

Conceptualization: M.Z., E.R.K., T.M.; Software: E.R.K., B.D., A.H.; Validation: M.Z.; Formal analysis: M.Z., E.R.K., B.D.; Investigation: M.Z., J.Z., O.M., A.H.; Resources: C.L., E.D.L., J.G., T.M.; Data curation: E.R.K.; Writing - original draft: M.Z.; Writing - review & editing: M.Z., E.R.K., O.M., B.D., E.D.L., J.G., T.M.; Visualization: M.Z., E.R.K.; Supervision: C.L., E.D.L., J.G., T.M.; Funding acquisition: T.M.

Funding

This work, and M.Z., E.R.K. and J.Z., were supported by a grant from the Natural Sciences and Engineering Research Council of Canada (NSERC; 04248). T.M. is the recipient of Career Awards from the Michael Smith Foundation for Health Research, and M.Z. is the recipient of a Natural Sciences and Engineering Research Council of Canada Alexander Graham Bell Canada Graduate Scholarship - Doctoral and the Killam Doctoral Scholarship. E.D.L., O.M. and B.D. were supported by the Israel Science Foundation (1452/18), by the European Research Council (ERC) under the European Union's Horizon 2020 research and innovation program (grant agreement No. 819318) and by a research grant from A.-M. Boucher. E.D.L. is incumbent of the Recanati Career Development Chair of Cancer Research.

Data availability

All raw proteomics data have been deposited to the ProteomeXchange Consortium through the PRIDE partner repository with the identifier PXD012631.

Supplementary information

Supplementary information available online at https://jcs.biologists.org/lookup/doi/10.1242/jcs.244657.supplemental

Peer review history
The peer review history is available online at
https://jcs.biologists.org/lookup/doi/10.1242/jcs.244657.reviewer-comments.pdf

References

Alberti, S., Gladfelter, A. and Cell, M.-T. (2019). Considerations and challenges in studying liquid-liquid phase separation and biomolecular condensates. *Cell* **176**, 419-434. doi:10.1016/j.cell.2018.12.035

Albu, R. F., Chan, G. T., Zhu, M., Wong, E., Taghizadeh, F., Hu, X., Mehran, A. E., Johnson, J. D., Gsponer, J. and Mayor, T. (2015). A feature analysis of lower solubility proteins in three eukaryotic systems. *J. Proteomics* **118**, 21-38. doi:10.1016/j.jprot.2014.10.011

Bailey, T. L., Boden, M., Buske, F. A., Frith, M., Grant, C. E., Clementi, L., Ren, J., Li, W. W. and Noble, W. S. (2009). MEME Suite: tools for motif discovery and searching. *Nucleic Acids Res.* **37**, W202-W208. doi:10.1093/nar/gkp335

Bauer, D. F. (1972). Constructing confidence sets using rank statistics. *J. Am. Stat. Assoc.* **67**, 687-690. doi:10.1080/01621459.1972.10481279

Beckmann, B. M., Horos, R., Fischer, B., Castello, A., Eichelbaum, K., Alleaume, A.-M., Schwarzl, T., Curk, T., Foehr, S., Huber, W. et al. (2015). The RNA-binding proteomes from yeast to man harbour conserved enigmRBPs. *Nat. Commun.* **6**, 10127. doi:10.1038/ncomms10127

Buchan, R. J. and Parker, R. (2009). Eukaryotic stress granules: the ins and outs of translation. *Mol. Cell* **36**, 932-941. doi:10.1016/j.molcel.2009.11.020

Cherkasov, V., Hofmann, S., Druffel-Augustin, S., Mogk, A., Tyedmers, J., Stoecklin, G. and Bukau, B. (2013). Coordination of translational control and protein homeostasis during severe heat stress. *Curr. Biol.* **23**, 2452-2462. doi:10.1016/j.cub.2013.09.058

Cherkasov, V., Grousl, T., Theer, P., Vainshtein, Y., Gläßer, C., Mongis, C., Kramer, G., Stoecklin, G., Knop, M., Mogk, A. et al. (2015). Systemic control of protein synthesis through sequestration of translation and ribosome biogenesis factors during severe heat stress. *FEBS Lett.* **589**, 3654-3664. doi:10.1016/j.febslet.2015.10.010

Chong, P. A., Vernon, R. M. and Forman-Kay, J. D. (2018). RGG/RG Motif Regions in RNA Binding and Phase Separation. *J. Mol. Biol.* **430**, 4650-4665. doi:10.1016/j.jmb.2018.06.014

Decker, C. J., Teixeira, D. and Parker, R. (2007). Edc3p and a glutamine/asparagine-rich domain of Lsm4p function in processing body assembly in Saccharomyces cerevisiae. *J. Cell Biol.* **179**, 437-449. doi:10.1083/jcb.200704147

Deutsch, E. W., Csordas, A., Sun, Z., Jarnuczak, A., Perez-Riverol, Y., Ternent, T., Campbell, D. S., Bernal-Llinares, M., Okuda, S., Kawano, S. et al. (2017). The ProteomeXchange consortium in 2017: supporting the cultural change in proteomics public data deposition. *Nucleic Acids Res.* **45**, D1100-D1106. doi:10.1093/nar/gkw936

Escusa-Toret, S., Vonk, W. I. and Frydman, J. (2013). Spatial sequestration of misfolded proteins by a dynamic chaperone pathway enhances cellular fitness during stress. *Nat. Cell Biol.* **15**, 1231-1243. doi:10.1038/ncb2838

Fan, A. C. and Leung, A. K. L. (2016). RNA Processing. *Adv. Exp. Med. Biol.* **907**, 263-296. doi:10.1007/978-3-319-29073-7_11

Fang, N. N., Ng, A. H., Measday, V. and Mayor, T. (2011). Hul5 HECT ubiquitin ligase plays a major role in the ubiquitylation and turnover of cytosolic misfolded proteins. *Nat. Cell Biol.* **13**, 1344. doi:10.1038/ncb2343

Fang, N. N., Zhu, M., Rose, A., Wu, K.-P. and Mayor, T. (2016). Deubiquitinase activity is required for the proteasomal degradation of misfolded cytosolic proteins upon heat-stress. *Nat. Commun.* **7**, 12907. doi:10.1038/ncomms12907

Farny, N. G., Kedersha, N. L. and Silver, P. A. (2009). Metazoan stress granule assembly is mediated by P-eIF2α-dependent and -independent mechanisms. *RNA* **15**, 1814-1821. doi:10.1261/rna.1684009

Franzmann, T. M., Jahnel, M., Pozniakovsky, A., Mahamid, J., Holehouse, A. S., Nüske, E., Richter, D., Baumeister, W., Grill, S. W., Pappu, R. V. et al. (2018). Phase separation of a yeast prion protein promotes cellular fitness. *Science* **359**, eaao5654. doi:10.1126/science.aao5654

Ghosh, K. and Dill, K. (2010). Cellular proteomes have broad distributions of protein stability. *Biophys. J.* **99**, 3996-4002. doi:10.1016/j.bpj.2010.10.036

Gilks, N., Kedersha, N., Ayodele, M., Shen, L., Stoecklin, G., Dember, L. M. and Anderson, P. (2004). Stress granule assembly is mediated by prion-like aggregation of TIA-1. *Mol. Biol. Cell* **15**, 5383-5398. doi:10.1091/mbc.e04-08-0715

Grousl, T., Ivanov, P., Frydlová, I., Vašicová, P., Janda, F., Vojtová, J., Malínská, K., Malcová, I., Nováková, L., Janošková, D. et al. (2009). Robust heat shock induces eIF2α-phosphorylation-independent assembly of stress granules containing eIF3 and 40S ribosomal subunits in budding yeast, Saccharomyces cerevisiae. *J. Cell Sci.* **122**, 2078-2088. doi:10.1242/jcs.045104

Harrison, P. M. (2017). fLPS: Fast discovery of compositional biases for the protein universe. *BMC Bioinformatics* **18**, 476. doi:10.1186/s12859-017-1906-3

Hennig, S., Kong, G., Mannen, T., Sadowska, A., Kobelke, S., Blythe, A., Knott, G. J., Iyer, S. K., Ho, D., Newcombe, E. A. et al. (2015). Prion-like domains in RNA binding proteins are essential for building subnuclear paraspeckles. *J. Cell Biol.* **210**, 529-539. doi:10.1083/jcb.201504117

Huang, K.-Y., Su, M.-G., Kao, H.-J., Hsieh, Y.-C., Jhong, J.-H., Cheng, K.-H., Huang, H.-D. and Lee, T.-Y. (2016). dbPTM 2016: 10-year anniversary of a resource for post-translational modification of proteins. *Nucleic Acids Res.* **44**, D435-D446. doi:10.1093/nar/gkv1240

Huh, W.-K., Falvo, J. V., Gerke, L. C., Carroll, A. S., Howson, R. W., Weissman, J. S. and O'Shea, E. K. (2003). Global analysis of protein localization in budding yeast. *Nature* **425**, 686. doi:10.1038/nature02026

Hyman, A. A., Weber, C. A. and Jülicher, F. (2014). Liquid-liquid phase separation in biology. *Annu. Rev. Cell Dev. Biol.* **30**, 39-58. doi:10.1146/annurev-cellbio-100913-013325

Jain, S., Wheeler, J. R., Walters, R. W., Agrawal, A., Barsic, A. and Parker, R. (2016). ATPase-modulated stress granules contain a diverse proteome and substructure. *Cell* **164**, 487-498. doi:10.1016/j.cell.2015.12.038

Jones, D. T. and Cozzetto, D. (2015). DISOPRED3: precise disordered region predictions with annotated protein-binding activity. *Bioinformatics* **31**, 857-863. doi:10.1093/bioinformatics/btu744

Kato, M., Han, T. W., Xie, S., Shi, K., Du, X., Wu, L. C., Mirzaei, H., Goldsmith, E. J., Longgood, J., Pei, J. et al. (2012). Cell-free formation of RNA granules: low complexity sequence domains form dynamic fibers within hydrogels. *Cell* **149**, 753-767. doi:10.1016/j.cell.2012.04.017

Kedersha, N. L., Gupta, M., Li, W., Miller, I. and Anderson, P. (1999). RNA-binding proteins Tia-1 and Tiar link the phosphorylation of Eif-2α to the assembly of mammalian stress granules. *J. Cell Biol.* **147**, 1431-1442. doi:10.1083/jcb.147.7.1431

Kedersha, N., Stoecklin, G., Ayodele, M., Yacono, P., Lykke-Andersen, J., Fritzler, M. J., Scheuner, D., Kaufman, R. J., Golan, D. E. and Anderson, P. (2005). Stress granules and processing bodies are dynamically linked sites of mRNP remodeling. *J. Cell Biol.* **169**, 871-884. doi:10.1083/jcb.200502088

Khong, A., Matheny, T., Jain, S., Mitchell, S. F., Wheeler, J. R. and Parker, R. (2017). The stress granule transcriptome reveals principles of mRNA accumulation in stress granules. *Mol. Cell* **68**, 808-820.e5. doi:10.1016/j.molcel.2017.10.015

Kimball, S. R., Horetsky, R. L., Ron, D., Jefferson, L. S. and Harding, H. P. (2003). Mammalian stress granules represent sites of accumulation of stalled translation initiation complexes. *Am. J. Physiol.Cell. Ph.* **284**, C273-C284. doi:10.1152/ajpcell.00314.2002

Koh, J., Chong, Y., Friesen, H., Moses, A., Boone, C., Andrews, B. and Moffat, J. (2015). CYCLoPs: A comprehensive database constructed from automated analysis of protein abundance and subcellular localization patterns in saccharomyces cerevisiae. *G3 Genes Genomes Genetics* **5**, 1223-1232. doi:10.1534/g3.115.017830

Kroschwald, S., Maharana, S., Mateju, D., Malinovska, L., Nüske, E., Poser, I., Richter, D. and Alberti, S. (2015). Promiscuous interactions and protein disaggregases determine the material state of stress-inducible RNP granules. *eLife* **4**, e06807. doi:10.7554/eLife.06807

Kroschwald, S., Munder, M. C., Maharana, S., Franzmann, T. M., Richter, D., Ruer, M., Hyman, A. A. and Alberti, S. (2018). Different material states of Pub1 condensates define distinct modes of stress adaptation and recovery. *Cell Reports* **23**, 3327-3339. doi:10.1016/j.celrep.2018.05.041

Kuechler, E. R., Budzyńska, P. M., Bernardini, J. P., Gsponer, J. and Mayor, T. (2020). Distinct features of stress granule proteins predict localization in membraneless organelle. *J. Mol. Biol.* **432**, 2349-2368. doi:10.1016/j.jmb.2020.02.020

Kyte, J. and Doolittle, R. F. (1982). A simple method for displaying the hydropathic character of a protein. *J. Mol. Biol.* **157**, 105-132. doi:10.1016/0022-2836(82)90515-0

Lancaster, A. K., Nutter-Upham, A., Lindquist, S. and King, O. D. (2014). PLAAC: a web and command-line application to identify proteins with prion-like amino acid composition. *Bioinformatics* **30**, 2501-2502. doi:10.1093/bioinformatics/btu310

Lechler, M. C., Crawford, E. D., Groh, N., Widmaier, K., Jung, R., Kirstein, J., Trinidad, J. C., Burlingame, A.L. and David, D.C. (2017). Reduced insulin/IGF-1 signaling restores the dynamic properties of key stress granule Proteins during aging. *Cell Reports* **18**, 454-467. doi:10.1016/j.celrep.2016.12.033

Leuenberger, P., Ganscha, S., Kahraman, A., Cappelletti, V., Boersema, P. J., von Mering, C., Claassen, M. and Picotti, P. (2017). Cell-wide analysis of protein thermal unfolding reveals determinants of thermostability. *Science* **355**, eaai7825 doi:10.1126/science.aai7825

Li, K., Zhao, K., Ossareh-Nazari, B., Da, G., Dargemont, C. and Marmorstein, R. (2005). Structural basis for interaction between the Ubp3 deubiquitinating enzyme and its Bre5 cofactor. *J. Biol. Chem.* **280**, 29176-29185. doi:10.1074/jbc.M502975200

Li, K., Ossareh-Nazari, B., Liu, X., Dargemont, C. and Marmorstein, R. (2007). Molecular basis for Bre5 cofactor recognition by the Ubp3 deubiquitylating enzyme. *J. Mol. Biol.* **372**, 194-204. doi:10.1016/j.jmb.2007.06.052

Lin, Y., Protter, D., Rosen, M. K. and Parker, R. (2015). Formation and maturation of phase-separated liquid droplets by RNA-binding proteins. *Mol. Cell* **60**, 208-219. doi:10.1016/j.molcel.2015.08.018

Linding, R., Schymkowitz, J., Rousseau, F., Diella, F. and Serrano, L. (2004). A comparative study of the relationship between protein structure and β-aggregation

in globular and intrinsically disordered proteins. *J. Mol. Biol.* **342**, 345-353. doi:10.1016/j.jmb.2004.06.088

Li, P., Banjade, S., Cheng, H.-C., Kim, S., Chen, B., Guo, L., Llaguno, M., Hollingsworth, J. V., King, D. S., Banani, S. F. et al. (2012). Phase transitions in the assembly of multivalent signalling proteins. *Nature* **483**, 336. doi:10.1038/nature10879

Magnan, C. N. and Baldi, P. (2014). SSpro/ACCpro 5: almost perfect prediction of protein secondary structure and relative solvent accessibility using profiles, machine learning and structural similarity. *Bioinformatics* **30**, 2592-2597. doi:10.1093/bioinformatics/btu352

Malhis, N., Wong, E. T. C., Nassar, R. and Gsponer, J. (2015). Computational identification of MoRFs in protein sequences using hierarchical application of bayes rule. *PLoS ONE* **10**, e0141603. doi:10.1371/journal.pone.0141603

Markmiller, S., Soltanieh, S., Server, K. L., Mak, R., Jin, W., Fang, M. Y., Luo, E.-C., Krach, F., Yang, D., Sen, A. et al. (2018). Context-dependent and disease-specific diversity in protein interactions within stress granules. *Cell* **172**, 590-604.e13. doi:10.1016/j.cell.2017.12.032

Matalon, O., Steinberg, A., Sass, E., Hausser, J. and Levy, E. D. (2018). Reprogramming protein abundance fluctuations in single cells by degradation. *Biorxiv*, 260695. doi:10.1101/260695

Mateju, D., Franzmann, T. M., Patel, A., Kopach, A., Boczek, E. E., Maharana, S., Lee, H. O., Carra, S., Hyman, A. A. and Alberti, S. (2017). An aberrant phase transition of stress granules triggered by misfolded protein and prevented by chaperone function. *EMBO J.* **36**, 1669-1687. doi:10.15252/embj.201695957

McLeay, R. C. and Bailey, T. L. (2010). Motif enrichment analysis: a unified framework and an evaluation on ChIP data. *BMC Bioinformatics* **11**, 165. doi:10.1186/1471-2105-11-165

Mitrea, D. M. and Kriwacki, R. W. (2016). Phase separation in biology; functional organization of a higher order. *Cell Commun. Signal.* **14**, 1. doi:10.1186/s12964-015-0125-7

Mitrea, D. M., Cika, J. A., Stanley, C. B., Nourse, A., Onuchic, P. L., Banerjee, P. R., Phillips, A. H., Park, C.-G., Deniz, A. A. and Kriwacki, R. W. (2018). Self-interaction of NPM1 modulates multiple mechanisms of liquid–liquid phase separation. *Nat. Commun.* **9**, 842. doi:10.1038/s41467-018-03255-3

Mittag, T. and Parker, R. (2018). Multiple modes of protein-protein interactions promote RNP granule assembly. *J. Mol. Biol.* **430**, 4636-4649. doi:10.1016/j.jmb.2018.08.005

Molliex, A., Temirov, J., Lee, J., Coughlin, M., Kanagaraj, A. P., Kim, H. J., Mittag, T. and Taylor, J. P. (2015). Phase separation by low complexity domains promotes stress granule assembly and drives pathological fibrillization. *Cell* **163**, 123-133. doi:10.1016/j.cell.2015.09.015

Nostramo, R., Varia, S. N., Zhang, B., Emerson, M. M. and Herman, P. K. (2016). The catalytic activity of the Ubp3 deubiquitinating protease is required for efficient stress granule assembly in saccharomyces cerevisiae. *Mol. Cell. Biol.* **36**, 173-183. doi:10.1128/MCB.00609-15

Pak, C. W., Kosno, M., Holehouse, A. S., Padrick, S. B., Mittal, A., Ali, R., Yunus, A. A., Liu, D. R., Pappu, R. V. and Rosen, M. K. (2016). Sequence determinants of intracellular phase separation by complex coacervation of a disordered protein. *Mol. Cell* **63**, 72-85. doi:10.1016/j.molcel.2016.05.042

Park, S.-H., Kukushkin, Y., Gupta, R., Chen, T., Konagai, A., Hipp, M. S., Hayer-Hartl, M. and Hartl, F. U. (2013). PolyQ proteins interfere with nuclear degradation of cytosolic proteins by sequestering the Sis1p chaperone. *Cell* **154**, 134-145. doi:10.1016/j.cell.2013.06.003

Patel, A., Lee, H. O., Jawerth, L., Maharana, S., Jahnel, M., Hein, M. Y., Stoynov, S., Mahamid, J., Saha, S., Franzmann, T. M. et al. (2015). A liquid-to-solid phase transition of the ALS protein FUS accelerated by disease mutation. *Cell* **162**, 1066-1077. doi:10.1016/j.cell.2015.07.047

Protter, D., Rao, B. S., Treeck, B., Lin, Y., Mizoue, L., Rosen, M. K. and Parker, R. (2018). Intrinsically disordered regions can contribute promiscuous interactions to RNP granule assembly. *Cell Reports* **22**, 1401-1412. doi:10.1016/j.celrep.2018.01.036

Rao, B. S. and Parker, R. (2017). Numerous interactions act redundantly to assemble a tunable size of P bodies in Saccharomyces cerevisiae. *Proc. Natl. Acad. Sci. USA* **114**, E9569-E9578. doi:10.1073/pnas.1712396114

Reineke, L. C., Dougherty, J. D., Pierre, P. and Lloyd, R. E. (2012). Large G3BP-induced granules trigger eIF2α phosphorylation. *Mol. Biol. Cell* **23**, 3499-3510. doi:10.1091/mbc.e12-05-0385

Reineke, L. C., Tsai, W.-C., Jain, A., Kaelber, J. T., Jung, S. Y. and Lloyd, R. E. (2017). Casein kinase 2 is linked to stress granule dynamics through phosphorylation of the stress granule nucleating protein G3BP1. *Mol. Cell. Biol.* **37**, e00596-e00516. doi:10.1128/MCB.00596-16

Riback, J. A., Katanski, C. D., Kear-Scott, J. L., Pilipenko, E. V., Rojek, A. E., Sosnick, T. R. and Drummond, D. A. (2017). Stress-triggered phase separation is an adaptive, evolutionarily tuned response. *Cell* **168**, 1028-1040.e19. doi:10.1016/j.cell.2017.02.027

Richter, K., Haslbeck, M. and Buchner, J. (2010). The heat shock response: life on the verge of death. *Mol. Cell* **40**, 253-266. doi:10.1016/j.molcel.2010.10.006

Saad, S., Cereghetti, G., Feng, Y., Picotti, P., Peter, M. and Dechant, R. (2017). Reversible protein aggregation is a protective mechanism to ensure cell cycle restart after stress. *Nat. Cell Biol.* **19**, 1202-1213. doi:10.1038/ncb3600

Schindelin, J., Arganda-Carreras, I., Frise, E., Kaynig, V., Longair, M., Pietzsch, T., Preibisch, S., Rueden, C., Saalfeld, S., Schmid, B. et al. (2012). Fiji: an open-source platform for biological-image analysis. *Nat. Methods* **9**, 676. doi:10.1038/nmeth.2019

Shevchenko, A., Wilm, M., Vorm, O., Jensen, O. N., Podtelejnikov, A. V., Neubauer, G., Shevchenko, A., Mortensen, P. and Mann, M. (1996). A strategy for identifying gel-separated proteins in sequence databases by MS alone. *Biochem. Soc. T.* **24**, 893-896. doi:10.1042/bst0240893

Specht, S., Miller, S. B. M., Mogk, A. and Bukau, B. (2011). Hsp42 is required for sequestration of protein aggregates into deposition sites in Saccharomyces cerevisiae. *J. Cell Biol.* **195**, 617-629. doi:10.1083/jcb.201106037

Thedieck, K., Holzwarth, B., Prentzell, M. T., Boehlke, C., Kläsener, K., Ruf, S., Sonntag, A. G., Maerz, L., Grellscheid, S.-N., Kremmer, E. et al. (2013). Inhibition of mTORC1 by astrin and stress granules prevents apoptosis in cancer cells. *Cell* **154**, 859-874. doi:10.1016/j.cell.2013.07.031

Turoverov, K., Kuznetsova, I., Fonin, A. V., Darling, A. L., Zaslavsky, B. Y. and Uversky, V. N. (2019). Stochasticity of biological soft matter: emerging concepts in intrinsically disordered proteins and biological phase separation. *Trends Biochem. Sci.* **44**, 716-728. doi:10.1016/j.tibs.2019.03.005

Udeshi, N. D., Mertins, P., Svinkina, T. and Carr, S. A. (2013). Large-scale identification of ubiquitination sites by mass spectrometry. *Nat. Protoc.* **8**, 1950-1960. doi:10.1038/nprot.2013.120

Vizcaíno, J. A., Deutsch, E. W., Wang, R., Csordas, A., Reisinger, F., Ríos, D., Dianes, J. A., Sun, Z., Farrah, T., Bandeira, N. et al. (2014). ProteomeXchange provides globally coordinated proteomics data submission and dissemination. *Nat. Biotechnol.* **32**, 223-226. doi:10.1038/nbt.2839

Wallace, E. W., Kear-Scott, J. L., Pilipenko, E. V., Schwartz, M. H., Laskowski, P. R., Rojek, A. E., Katanski, C. D., Riback, J. A., Dion, M. F., Franks, A. M. et al. (2015). Reversible, specific, active aggregates of endogenous proteins assemble upon heat stress. *Cell* **162**, 1286-1298. doi:10.1016/j.cell.2015.08.041

Wang, M., Herrmann, C. J., Simonovic, M., Szklarczyk, D. and von Mering, C. (2015). Version 4.0 of PaxDb: protein abundance data, integrated across model organisms, tissues, and cell-lines. *Proteomics* **15**, 3163-3168. doi:10.1002/pmic.201400441

Yoon, J.-H., Choi, E.-J. and Parker, R. (2010). Dcp2 phosphorylation by Ste20 modulates stress granule assembly and mRNA decay in Saccharomyces cerevisiae. *J. Cell Biol.* **189**, 813-827. doi:10.1083/jcb.200912019

Youn, J.-Y., Dunham, W. H., Hong, S. J., Knight, J. D. R., Bashkurov, M., Chen, G. I., Bagci, H., Rathod, B., MacLeod, G., Eng, S. W. M. et al. (2018). High-density proximity mapping reveals the subcellular organization of mrna-associated granules and bodies. *Mol. Cell* **69**, 517-532.e11. doi:10.1016/j.molcel.2017.12.020

Youn, J.-Y., Dyakov, B. J. A., Zhang, J., Knight, J. D. R., Vernon, R. M., Forman-Kay, J. D. and Gingras, A.-C. (2019). Properties of stress granule and P-body proteomes. *Mol. Cell* **76**, 286-294. doi:10.1016/j.molcel.2019.09.014